Robust and high-fidelity nondestructive Rydberg parity meter

Ri-Hua Zheng,[1,2] Yi-Hao Kang,[1,2] S.-L. Su,[3,*] Jie Song,[4] and Yan Xia[1,2,†]

[1]*Department of Physics, Fuzhou University, Fuzhou 350116, China*

[2]*Fujian Key Laboratory of Quantum Information and Quantum Optics (Fuzhou University), Fuzhou 350116, China*

[3]*School of Physics, Zhengzhou University, Zhengzhou 450001, China*

[4]*Department of Physics, Harbin Institute of Technology, Harbin 150001, China*

(Received 5 March 2020; revised 26 April 2020; accepted 12 June 2020; published 6 July 2020)

In this paper, we propose a robust and high-fidelity scheme to construct a nondestructive Rydberg parity meter by optimized inverse engineering, after which we can know the parity information of the bipartite state without destroying it, implying that the output bipartite state can be further used in the rest quantum information processing tasks. Specifically speaking, we build a model with two systematic Rydberg atoms and one auxiliary Rydberg atom and control them by utilizing optimized inverse engineering against systematic error. Also, since the accumulated time for the Rydberg atoms simultaneously being in Rydberg states is minimized, the mechanical effect and the further possible ionization are almost avoided. Moreover, numerical simulation shows that the present scheme is robust against the systematic error, the dephasing, and the thermal noise, demonstrating feasibility in the experiment.

DOI: 10.1103/PhysRevA.102.012609

I. INTRODUCTION

Parity meters, which are used to distinguish whether a quantum state has even or odd parity, have been widely applied in various parts of quantum information processing (QIP), such as purifying entangled states [1], realizing quantum computation [2,3], generating entangled states analysis [4], and further applying it to quantum teleportation [5–7]. Implementing a conventional parity meter destroys the parity state, causing a waste of quantum entanglement resource. To solve this problem and boost efficiency of the QIP, the nondestructive parity meter was developed on several kinds of platforms, such as optical systems [3,8,9] and spin systems [10], giving researchers a prospect for increasing the diversity of platforms for nondestructive parity meters.

Among various systems for implementing the QIP, the Rydberg atom system is a promising one and offers a relatively long coherence time [11–14], which is of value for achieving the nondestructive parity meter. The long-range Rydberg-Rydberg interaction (RRI) [13–15] among neutral atoms induces interesting peculiar phenomena, such as Rydberg blockade [11,12,16,17] and Rydberg antiblockade [18–23]. Rydberg blockade stipulates that, once an atom is excited to Rydberg state, the other atoms will all be blocked in ground states when resonant Rabi frequencies are much smaller than the energy shift of the RRI. Such a phenomenon has been widely used in QIP, such as quantum computation [24–27] and preparation of quantum entanglement [28–32]. On the contrary, if the Rabi frequencies are not resonant, with huge two-photon detunings closed to the energy shift of the RRI, an opposite phenomenon occurs, called Rydberg antiblockade, yielding more than one atom pumping to Rydberg states. The Rydberg antiblockade is also used to generate entanglement [33–37]. In a word, the Rydberg atom is a promising platform in quantum information science.

Recently, a parity meter based on many-body Rydberg atoms was demonstrated experimentally [38] to measure the bound of a GHZ entangled state generated by optimal control pulses, demonstrating a promising approach for the deterministic creation and manipulation of large-scale entangled states. Moreover, the four-body Rydberg parity were employed for building a Hamiltonian with the Lechner-Hauke-Zoller architecture in a quantum annealer [39] in the experiment. On that basis, Ref. [40] proposed a scheme for construction of a nondestructive parity meter on the platform of the Rydberg atom, which explored a new path to Rydberg-atom-based QIP. Nevertheless, the scheme of Ref. [40] may suffer from technical limitations and parameter deviation. More specifically, since more than one Rydberg atom is populated at the same time, the mechanical effect [41] would be induced and cause further ionization of Rydberg atoms [41–43]. Therefore, it makes sense to build a nondestructive Rydberg parity meter (NRPM) with a more robust way, i.e., overcoming possible drawbacks of simultaneous excitation of Rydberg atoms and parameter deviation.

To surmount the drawbacks mentioned above, in this paper, we propose an experimentally feasible scheme to construct a two-qubit NRPM with high fidelity, which is robust against the mechanical effect and parameter deviation. For a two-qubit system, a nondestructive parity meter can evolve a general initial state $|\psi_0\rangle = \mathcal{N}(\alpha_1|00\rangle + \alpha_2|01\rangle + \alpha_3|10\rangle + \alpha_4|11\rangle)$ [here $\mathcal{N} = 1/(\sum_{q=1}^{4}|\alpha_q|^2)^{1/2}$] into either an even-parity final state $|\psi_{\text{even}}\rangle = \mathcal{N}_1(\alpha_1|00\rangle + \alpha_4|11\rangle)$ or an odd-parity final state $|\psi_{\text{odd}}\rangle = \mathcal{N}_2(\alpha_2|01\rangle + \alpha_3|10\rangle)$ with $\mathcal{N}_1 = 1/(|\alpha_1|^2 + |\alpha_4|^2)^{1/2}$ and $\mathcal{N}_2 = 1/(|\alpha_2|^2 + |\alpha_3|^2)^{1/2}$. The configuration of the present scheme consists of three Rydberg atoms: two systematic atoms and one auxiliary atom trapped in fixed position, as a triangle, with the RRI between each

*slsu@zzu.edu.cn

†xia-208@163.com

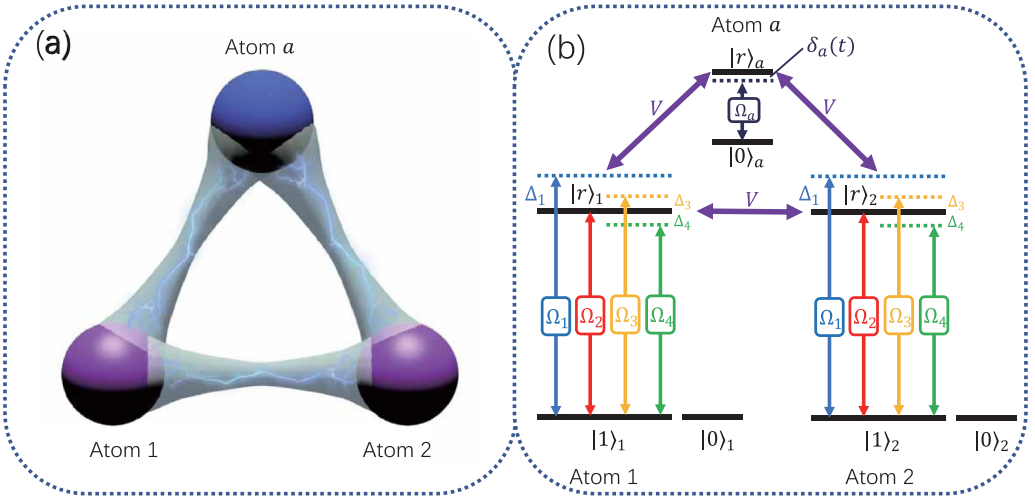

FIG. 1. (a) Schematic of model of the robust and high-fidelity NRPM. (b) Energy levels for atoms 1, 2, and a.

pair of them. To avoid the simultaneous excitation of Rydberg atoms, an unconventional Rydberg pumping (URP) [44], different from both the Rydberg blockade and the Rydberg antiblockade, is considered here. That is, two atoms in different ground states will be excited to a single Rydberg state, but be stable when in the same ground states. We modified the original URP model with two extra Rabi frequencies, which makes the control of evolution more feasible, and apply the modified URP model to the systematic atoms. Additionally, the auxiliary atom is pumped by a classical pulse with small detuning, i.e., utilizing the Rydberg blockade, to ensure there is no simultaneous excitation of Rydberg atoms during the evolution. Thus, the present scheme may have negligible mechanical effect in contrast with the scheme of Ref. [40].

In addition, another factor that affects the fidelity of the scheme in Ref. [40] in the experiment is parameter deviation, which is mainly caused by the systematic error and can be regarded as an effect driven by a perturbative Hamiltonian. The way to solve this problem is to properly minimize the sensitivity factor of the systematic error, depending on the coupling terms in time-dependent perturbation theory. Moreover, the minimization of the sensitivity factor will result in time-dependent properties of Rabi frequencies, which should also satisfy boundary conditions of specific population transformation. Therefore, we apply SU(2)-dynamic-based inverse engineering theory [27,45–57] and afterwards optimize it against systematic error to deal with possible parameters deviation in the experiment, consequently establishing an error-tolerant way to realize the NRPM. The numerical simulation indicates that the scheme is robust against both systematic error and decoherence caused by the thermal noise and the dephasing.

The paper is organized as follows: In Sec. II, we construct an effective two-level Hamiltonian for the two systematic atoms. In Sec. III, based on specific boundary conditions, we inversely design fields for the effective Hamiltonian, with optimization against systematic error. In Sec. IV, we describe detailed procedures for realizing the robust and high-fidelity NRPM. Next, we discuss the experimental feasibility and the conclusion in Secs. V and VI, respectively.

II. PHYSICAL MODEL FOR THE ROBUST AND HIGH-FIDELITY NONDESTRUCTIVE RYDBERG PARITY METER

In this section, we introduce the physical model for implementing a robust and high-fidelity NRPM. As shown in Fig. 1, three Rydberg atoms are equidistantly trapped as a triangle, each pair of which partake in the RRI with interaction energy V. Atom k ($k = 1, 2$) has two ground states $|0\rangle_k$ and $|1\rangle_k$, and one Rydberg state $|r\rangle_k$. The transition $|1\rangle_k \leftrightarrow |r\rangle_k$ is driven by four different classical fields with Rabi frequencies Ω_1, $\Omega_2(t)$, $\Omega_3(t)$, and $\Omega_4(t)$, whose blue detunings are Δ_1, 0, Δ_3, and $-\Delta_4$, respectively. In addition, the auxiliary atom a has one ground state $|0\rangle_a$ and one Rydberg state $|r\rangle_a$, which are coupled with Rabi frequency $\Omega_a(t)$ and time-dependent red detuning $\delta_a(t)$. The Hamiltonian of atoms 1 and 2 in the interaction picture is (assuming $\hbar = 1$ henceforward)

$$H_i(t) = \sum_{k=1}^{2}[\Omega_1 e^{-i\Delta_1 t} + \Omega_2(t) + \Omega_3(t)e^{-i\Delta_3 t} + \Omega_4(t)e^{i\Delta_4 t}]|r\rangle_k\langle 1| + \text{H.c.} + V|rr\rangle_{12}\langle rr|. \quad (1)$$

Under the conditions, $V = \Delta_1 \gg \Omega_1 \gg \Omega_2(t)$, $\Delta_3 = \Delta_4$, and $\{\Delta_3, \Delta_1 \pm \Delta_3, \Delta_1 - 2\Delta_3\} \gg \{\Omega_3(t), \Omega_4(t)\}$, the original Hamiltonian in Eq. (1) can be reduced to [see Appendix]

$$H'_{\text{eff}}(t) = \Omega_2(t)(|r0\rangle_{12}\langle 10| + |0r\rangle_{12}\langle 01|) + \text{H.c.} + \left(\frac{\Omega_3(t)^2}{\Delta_3} - \frac{\Omega_4(t)^2}{\Delta_3}\right)(2|11\rangle_{12}\langle 11| + |01\rangle_{12}\langle 01| + |10\rangle_{12}\langle 10| - |0r\rangle_{12}\langle 0r| - |r0\rangle_{12}\langle r0|), \quad (2)$$

with canceling Stark-shift terms in Ω_1. If we ignore the term $2(\frac{\Omega_3(t)^2}{\Delta_3} - \frac{\Omega_4(t)^2}{\Delta_3})|11\rangle_{12}\langle 11|$, which only induces the phase accumulation on state $|11\rangle_{12}$, Eq. (2) is simplified to

$$H'_{\text{eff}}(t) = \Omega_2(t)(|r0\rangle_{12}\langle 10| + |0r\rangle_{12}\langle 01|) + \text{H.c.} + \left(\frac{\Omega_3(t)^2}{\Delta_3} - \frac{\Omega_4(t)^2}{\Delta_3}\right)(|01\rangle_{12}\langle 01| + |10\rangle_{12}\langle 10| - |0r\rangle_{12}\langle 0r| - |r0\rangle_{12}\langle r0|). \quad (3)$$

The effective Hamiltonian shown in Eq. (3) can be divided into two subspaces, $\{|r0\rangle_{12}, |10\rangle_{12}\}$ and $\{|0r\rangle_{12}, |01\rangle_{12}\}$, with no crossover. Therefore, we can describe $H'_{\rm eff}(t)$ by a Hamiltonian with a SU(2) dynamic structure as

$$H'^{(2)}_{\rm eff}(t) = \Omega(t)|\zeta_1\rangle\langle\zeta_2| + \text{H.c.} + \delta(t)(|\zeta_1\rangle\langle\zeta_1| - |\zeta_2\rangle\langle\zeta_2|), \tag{4}$$

with $\Omega(t) = \Omega_2(t)$, $\delta(t) = \frac{\Omega_3(t)^2}{\Delta_3} - \frac{\Omega_4(t)^2}{\Delta_3}$, and basis $\{|\zeta_1\rangle, |\zeta_2\rangle\}$ being $\{|10\rangle_{12}, |r0\rangle_{12}\}$ or $\{|01\rangle_{12}, |0r\rangle_{12}\}$.

III. OPTIMIZATION OF INVERSE ENGINEERING AGAINST SYSTEMATIC ERROR

In Sec. II, we simplified the Hamiltonian of atoms 1 and 2 into a two-level Hamiltonian, with the SU(2) dynamic structure. In this section, on the basis of the derived two-level Hamiltonian, we give a method for optimizing the inverse engineering, making it more robust against the systematic error and therefore increasing error-tolerant property for the NRPM in the experiment.

It is appropriate to primarily apply inverse engineering [58,59] to deal with the two-level effective Hamiltonian, described as

$$H'^{(2)}_{\rm eff}(t) = \begin{pmatrix} \delta(t) & \Omega(t) \\ \Omega(t) & -\delta(t) \end{pmatrix} = \Omega(t)\sigma_x + \delta(t)\sigma_z. \tag{5}$$

The Schrödinger equation is written as

$$i\partial_t|\psi(t)\rangle = H'^{(2)}_{\rm eff}(t)|\psi(t)\rangle. \tag{6}$$

For inversely designing suitable $\Omega(t)$ and $\delta(t)$ to give desired dynamics, we perform a picture transformation as $R(t)^\dagger|\psi(t)\rangle = |\psi^R(t)\rangle$ by using $R(t)$, a general unitary transformation of a two-level system that is given by [47]

$$R(\theta, \eta, \xi) = \begin{pmatrix} e^{i\xi}\cos\theta & -e^{-i\eta}\sin\theta \\ e^{i\eta}\sin\theta & e^{-i\xi}\cos\theta \end{pmatrix}, \tag{7}$$

with θ, η, and ξ being time-dependent parameters. After transforming and setting $\eta = -\xi$, the Hamiltonian in the new picture can be written as

$$\begin{aligned} H^R(t) &= R^\dagger(t)H'^{(2)}_{\rm eff}(t)R(t) + i\partial_t R^\dagger(t)R(t) \\ &= \{\Omega(t)\cos(2\xi)\sin(2\theta) + \cos(2\theta)[\delta(t) + \dot\xi]\}\sigma_z \\ &\quad + \{\Omega(t)\cos(2\xi)\cos(2\theta) - \sin(2\theta)[\delta(t) + \dot\xi]\}\sigma_x \\ &\quad + [\Omega(t)\sin(2\xi) - \dot\theta]\sigma_y. \end{aligned} \tag{8}$$

For briefly deriving the evolution operator $U^R(t)$ in the present picture, we set $H^R(t) = f(t)\sigma_z$, leading to

$$\Omega(t) = \frac{\dot\theta}{\sin(2\xi)}, \quad \delta(t) = \dot\theta\cot(2\xi)\cot(2\theta) - \dot\xi, \tag{9}$$

and

$$f(t) = \frac{\dot\theta\cot(2\xi)}{\sin 2\theta}. \tag{10}$$

When condition in Eq. (9) is satisfied, it is clear to have $[H^R(t), H^R(t-dt)] = 0$, i.e., $[e^{-iH^R(t)dt}, e^{-iH^R(t-dt)}dt] = 0$, yielding

$$U^R(t) = e^{-i\int_0^t H^R(t')dt'} = e^{-i\gamma(t)\sigma_z}, \tag{11}$$

with $\gamma(t) = \int_0^t \frac{\dot\theta\cot(2\xi)}{\sin 2\theta}dt'$. Now we go back to the original picture in Eq. (6) and calculate the evolution operator

$$U'(t) = R(t)U^R(t)R^\dagger(0). \tag{12}$$

Because $R(t)$ is a unitary operator, obviously satisfying

$$R^\dagger(0)R(0) = \begin{pmatrix} 1 & 0 \\ 0 & 1 \end{pmatrix},$$

we set

$$R^\dagger(0) = \begin{pmatrix} e^{-i\pi/4} & 0 \\ 0 & e^{i\pi/4} \end{pmatrix}, \quad R(0) = \begin{pmatrix} e^{i\pi/4} & 0 \\ 0 & e^{-i\pi/4} \end{pmatrix}, \tag{13}$$

generating

$$U'(t) = \begin{pmatrix} e^{-i\gamma+i\xi-i\pi/4}\cos\theta & -e^{i\gamma+i\xi+i\pi/4}\sin\theta \\ e^{-i\gamma-i\xi-i\pi/4}\sin\theta & e^{i\gamma-i\xi+i\pi/4}\cos\theta \end{pmatrix}, \tag{14}$$

$\theta(0) = 0$, and $\xi(0) = \pi/4$. Here, if someone wants to transfer all the population from $|\zeta_1\rangle$ to $|\zeta_2\rangle$, i.e., $|\psi(0)\rangle = |\zeta_1\rangle$ and $|\psi(t_f)\rangle = e^{im}|\zeta_2\rangle$ (0 and t_f being the initial time and the final time, respectively, and e^{im} being an arbitrary phase), the evolution operator $U'(t)$ can be used to derive time-dependent state of the two-level system, $|\psi_1(t)\rangle$, such that

$$\begin{aligned} |\psi_1(t)\rangle &= U'(t)|\zeta_1\rangle = \begin{pmatrix} e^{-i\gamma+i\xi-i\pi/4}\cos\theta \\ e^{-i\gamma-i\xi-i\pi/4}\sin\theta \end{pmatrix} \\ &= e^{-i\gamma+i\xi-i\pi/4}\begin{pmatrix} \cos\theta \\ e^{-2i\xi}\sin\theta \end{pmatrix}. \end{aligned} \tag{15}$$

Note that $e^{-i\gamma+i\xi-i\pi/4}$ here is the global phase of $|\zeta_1\rangle$ and $|\zeta_2\rangle$, namely, being inessential. By choosing boundary conditions,

$$\theta(0) = 0, \quad \theta(t_f) = \pi/2, \quad \xi(0) = \xi(t_f) = \pi/4, \tag{16}$$

to construct suitable parameters $\theta(t)$ and $\xi(t)$, i.e., $\Omega(t)$ and $\delta(t)$, one can convert all the population in $|\zeta_1\rangle$ to $|\zeta_2\rangle$. Observe that condition $\xi(t_f) = \pi/4$ is not necessary, which just control the relative phase between $|\zeta_2\rangle$ and $|\zeta_1\rangle$, while it can build $\xi(0) = \xi(t_f) = \pi/4$, properly avoiding singularity caused by $\cot(2\xi)$ in the expressions of $\Omega(t)$ and $\delta(t)$ in Eq. (9).

Up to now, we have derived the inverse engineering for a two-level system with the SU(2) dynamic structure. However, the normal case in the experiment is that the value of $\Omega(t)$ may not be adjusted exactly along the derived expression, which would decrease the fidelity inevitably. To solve this problem, Refs. [60–64] have provided a method to optimize the inverse engineering with respect to the systematic error. On that basis, we assume the systematic error rate being β, i.e.,

$$\Omega^{\rm real}(t) = (1+\beta)\Omega(t), \tag{17}$$

where $\Omega^{\rm real}(t)$ is the experimental value of $\Omega(t)$. Therefore, the perturbation Hamiltonian resulting from the systematic error can be depicted solely as

$$H_\beta = \beta\begin{pmatrix} 0 & \Omega(t) \\ \Omega(t) & 0 \end{pmatrix}. \tag{18}$$

Recall the time-dependent theory up to $O(\beta^2)$, such that

$$|\psi(t_f)\rangle = |\psi_1(t_f)\rangle - i\int_0^{t_f} dtU'(t_f,t)H_\beta(t)|\psi_1(t)\rangle - \int_0^{t_f} dt\int_0^t dt'U'(t_f,t)H_\beta(t) \times U'(t,t')H_\beta(t')|\psi_1(t')\rangle + \cdots, \quad (19)$$

where $|\psi_1(t)\rangle$ is the unperturbed solution of the Schrödinger equation and $U'(t_f,t)$ is the unperturbed evolution operator, given by $U'(t_f,t) = \sum_{k=1}^2 |\psi_k(t_f)\rangle\langle\psi_k(t)|$. When the initial state is $|\zeta_1\rangle$, the unperturbed solution, $|\psi_1(t)\rangle$, can be written as

$$|\psi_1(t)\rangle = \begin{pmatrix} e^{-i\gamma+i\xi-i\pi/4}\cos\theta \\ e^{-i\gamma-i\xi-i\pi/4}\sin\theta \end{pmatrix}. \quad (20)$$

In this case, another solution $|\psi_2(t)\rangle$, is orthogonal to $|\psi_1(t)\rangle$ and can be derived as

$$|\psi_2(t)\rangle = U'(t,0)|\zeta_2\rangle = \begin{pmatrix} -e^{i\gamma+i\xi+i\pi/4}\sin\theta \\ e^{i\gamma-i\xi+i\pi/4}\cos\theta \end{pmatrix}. \quad (21)$$

The fidelity for being in the unperturbed state $|\psi_1(t)\rangle$ can be approximately calculated by

$$F \approx 1 - \left|\int_0^{t_f} dt\langle\psi_1(t)|H_\beta(t)|\psi_2(t)\rangle\right|^2. \quad (22)$$

According to Ref. [60], we define the systematic-error sensitivity as

$$q = -\frac{1}{2}\frac{\partial^2 F}{\partial\beta^2}\bigg|_{\beta=0}. \quad (23)$$

Substituting Eqs. (18) and (20)–(22) into Eq. (23), we have

$$q = \left|\int_0^{t_f} dt[e^{-2i\gamma-2i\xi}\dot\theta\csc 2\xi(e^{4i\xi}\cos^2\theta - \sin^2\theta)]\right|^2. \quad (24)$$

Consequently, by choosing suitable expressions of $\xi(t)$ and $\theta(t)$, we can make the value of q as small as possible or, better yet, zero. Although the analytical solution $q = 0$ is a little difficult to obtain, the numerical method can be used to get a relatively small value of q. Here, we assume

$$\theta(t) = \frac{\pi}{2}\sin^2(\pi t/2t_f),$$
$$\xi(t) = \frac{\pi}{4} + \frac{a_1}{2}\sin(2\theta) + \frac{a_2}{2}\sin(4\theta), \quad (25)$$

where a_1 and a_2 are two time-independent parameters controlling the value of q. Note also that the expressions of $\theta(t)$ and $\xi(t)$ satisfy boundary conditions shown in Eq. (16) and that $\xi(t)$ is a Fourier sequence of $\theta(t)$. Additionally, the values of a_1 and a_2 should be chosen to make $\xi(t)$ shift in the range $[0, \frac{\pi}{2}]$, which can avoid the singularity caused by $\cot(2\xi)$ in the expressions of $\Omega(t)$ and $\delta(t)$ in Eq. (9). The value of $q(t)$ versus a_1 and a_2 is plotted in Fig. 2(a). Combining the singularity versus a_1 and a_2 shown in Fig. 2(b), we pick out the point $a_1 = 1.34$ and $a_2 = 0$, leading to $q(t) = 2.0344 \times 10^{-4} \approx 0$. To know the quantitative effect of the optimization against the systematic error, the fidelities for converting $|\zeta_1\rangle$ into $e^{im}|\zeta_2\rangle$ versus the systematic error rate β are plotted in Fig. 3. We can see from Fig. 3 that, compared with the time-dependent-field driving and flat-pulse driving ($\frac{\pi}{2}$ pulse), the optimized inverse engineering is more robust against systematic error. Therefore, the optimization is effective and will produce higher fidelity. For instance, at point $\beta = 0.12$, we have $F_1 = 99.43\%$, $F_2 = 98.21\%$, and $F_3 = 95.25\%$.

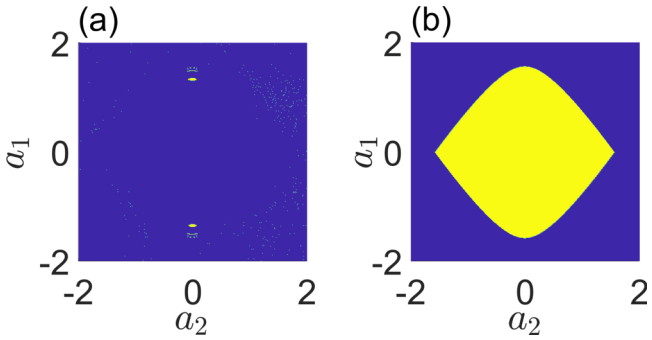

FIG. 2. (a) Value of $q(t)$ vs a_1 and a_2. Observe that here we display all the points which satisfy $q > 0.01$, by blue color, namely, the yellow points owning a range of [0, 0.01]. Such a disposition is innocuous because here we only want to find small-value points. (b) Singularity vs a_1 and a_2. The blue area is the forbidden zone and (a_1, a_2) located here will induce the singularity of $\Omega(t)$ and $\delta(t)$. On the other hand, points located in the yellow area will avoid the singularity of $\Omega(t)$ and $\delta(t)$.

In a word, one can add fields

$$\Omega(t) = \frac{\dot\theta}{\sin(2\xi)},$$
$$\delta(t) = \dot\theta\cot(2\xi)\cot(2\theta) - \dot\xi, \quad (26)$$

with

$$\theta(t) = \frac{\pi}{2}\sin^2(\pi t/2t_f),$$
$$\xi(t) = \frac{\pi}{4} + \frac{a_1}{2}\sin(2\theta) + \frac{a_2}{2}\sin(4\theta),$$
$$a_1 = 1.34, \quad a_2 = 0, \quad (27)$$

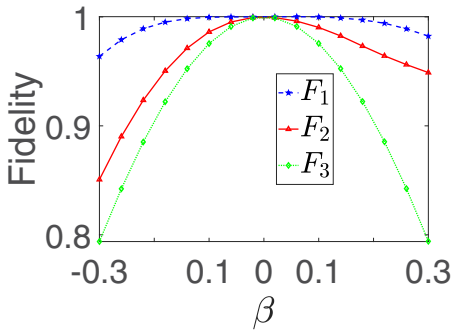

FIG. 3. Fidelities for transition $|\zeta_1\rangle \to e^{im}|\zeta_2\rangle$ vs the systematic error rate β, with F_1, F_2, and F_3 representing the fidelities of optimized inverse engineering, time-dependent-field driving, and flat-field driving, respectively. Note that the time-dependent-field driving corresponds to arbitrary choice of $\theta(t)$ and $\xi(t)$ [also satisfying the boundary conditions in Eq. (16)], for example, $\theta(t) = \pi\sin^2(\pi t/2t_f)/2$ and $\xi(t) = \pi/4 + \sin^2(\pi t/t_f)/2$. Also, the flat-field driving means using a $\frac{\pi}{2}$ pulse, i.e., $\Omega(t) = \pi/2$ and $\delta(t) = 0$.

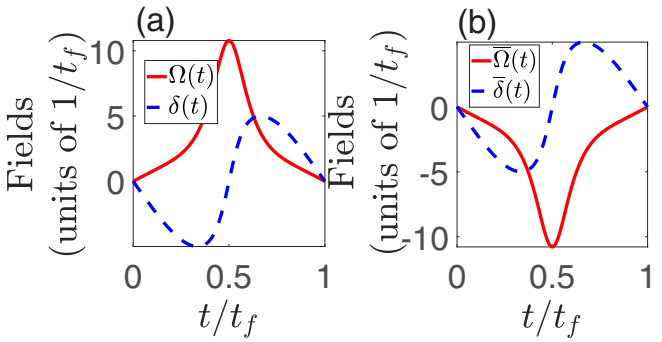

FIG. 4. (a) Fields for transition $|\zeta_1\rangle \to e^{im}|\zeta_2\rangle$. (b) Fields for transition $e^{im}|\zeta_2\rangle \to |\zeta_1\rangle$.

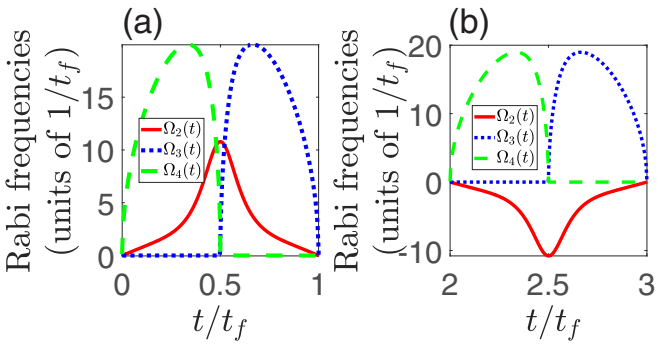

FIG. 5. (a) Rabi frequencies for transition $\mathcal{X}$. (b) Rabi frequencies for transition $\overline{\mathcal{X}}$. From Eq. (27) we can find that $\theta(t)+\theta(t_f-t)=\pi/2$ and then $\xi(t_f-t)=\xi(t)$, giving rise to $\overline{\delta}(t)=-\delta(t_f-t)=\delta(t)$ $[\delta(t)=\dot{\theta}\cot(2\xi)\cot(2\theta)-\dot{\xi}]$, which can be combined with Eq. (32) and leads to $\Omega_3(t-2t_f)=\Omega_3(t)$ and $\Omega_4(t-2t_f)=\Omega_4(t)$. This is why $\Omega_3(t)$ and $\Omega_4(t)$ in time interval $[0,t_f]$ look the same as $\Omega_3(t)$ and $\Omega_4(t)$ in time interval $[2t_f,3t_f]$, respectively.

to achieve transition $|\zeta_1\rangle \to e^{im}|\zeta_2\rangle$ in the two-level system. For the inverse transition, $e^{im}|\zeta_2\rangle \to |\zeta_1\rangle$, driven by Hamiltonian $\overline{H_{\rm eff}^{\prime(2)}}(t)$, the corresponding evolution operator $U''(t,0)$ will make the opposite contribution to $U'(t)$ (the evolution operator of forward transition), i.e., $U''(t,0)=U'^{\dagger}(t_f-t,t_f)$, leading to $\overline{H_{\rm eff}^{\prime(2)}}(t)=i\dot{U}''(t,0)U''^{\dagger}(t,0)=i\dot{U}'^{\dagger}(t_f-t,t_f)U'(t_f-t,t_f)=-H_{\rm eff}^{\prime(2)}(t_f-t)$. Therefore, the inverse transition, $e^{im}|\zeta_2\rangle \to |\zeta_1\rangle$, can be realized by adding fields, $\overline{\Omega}(t)=-\Omega(t_f-t)$ and $\overline{\delta}(t)=-\delta(t_f-t)$. The fields for transitions $|\zeta_1\rangle \to e^{im}|\zeta_2\rangle$ and $e^{im}|\zeta_2\rangle \to |\zeta_1\rangle$ in the two-level system are plotted in Figs. 4(a) and 4(b), respectively.

IV. PROCEDURES OF THE ROBUST AND HIGH-FIDELITY NONDESTRUCTIVE RYDBERG PARITY METER

We here depict the detailed procedures for implementing the robust and high-fidelity NRPM, including three steps:

Step 1. [for the time interval $t\in(0,t_f)$] Turn on pulses Ω_1, $\Omega_2(t)$, $\Omega_3(t)$, and $\Omega_4(t)$ of atoms 1 and 2. By using Eq. (4), the Rabi frequencies can be derived as [expressions of $\theta(t)$ and $\xi(t)$ shown in Eqs. (26) and (27)]

$$\Omega_2(t)=\Omega(t)=\frac{\dot{\theta}(t)}{\sin[2\xi(t)]},$$
$$\Omega_3(t)=\begin{cases}\sqrt{\Delta_3\delta(t)}, & \delta(t)\geqslant 0\\ 0, & \delta(t)<0,\end{cases}$$
$$\Omega_4(t)=\begin{cases}0, & \delta(t)\geqslant 0\\ \sqrt{-\Delta_3\delta(t)}, & \delta(t)<0,\end{cases} \tag{28}$$

and plot them $[t\in(0,t_f)]$ in Fig. 5(a). Observe that $\Omega_1=150/t_f$, $V=\Delta_1=2000/t_f$, and $\Delta_3=72/t_f$ are also chosen here and in Step 3 to guarantee the validity of the effective Hamiltonian in Eq. (4). In this case, we can make transition $\mathcal{X}$ (atoms 1 and 2 initially in ground states, and atom a initially in state $|0\rangle_a$):

$$\begin{aligned}&\mathcal{N}(\alpha_1|00\rangle_{12}+\alpha_2|01\rangle_{12}+\alpha_3|10\rangle_{12}+\alpha_4|11\rangle_{12})\otimes|0\rangle_a\\ &\quad\to\mathcal{N}[\alpha_1|00\rangle_{12}+e^{-i\gamma(t_f)-i\xi(t_f)-i\pi/4}(\alpha_2|0r\rangle_{12}\\ &\qquad+\alpha_3|r0\rangle_{12})+\alpha_4|11\rangle_{12}]\otimes|0\rangle_a,\end{aligned} \tag{29}$$

with α_1, α_2, α_3, and α_4 being arbitrary parameters and $\mathcal{N}$ being the normalization coefficient given by $\mathcal{N}=1/(|\alpha_1|^2+|\alpha_2|^2+|\alpha_3|^2+|\alpha_4|^2)^{1/2}$. In addition, $e^{-i\gamma(t_f)-i\xi(t_f)-i\pi/4}$ is the relative phase between $|0r(r0)\rangle_{12}$ and $|00\rangle_{12}$ or $|11\rangle_{12}$ [see Eq. (15)].

Step 2. [for the time interval $t\in(t_f,2t_f)$] Turn off the pulses Ω_1, $\Omega_2(t)$, $\Omega_3(t)$, and $\Omega_4(t)$ of atoms 1 and 2. Meanwhile, turn on the fields $\Omega_a(t)$ and $\delta_a(t)$ of atom a. Due to the Rydberg blockade ($V=2000/t_f$ here), terms like $|0r0\rangle_{12a}$ and $|r00\rangle_{12a}$ cannot be pumped to $|0rr\rangle_{12a}$ and $|r0r\rangle_{12a}$, respectively, while transitions $|010\rangle_{12a}\to|01r\rangle_{12a}$ and $|100\rangle_{12a}\to|10r\rangle_{12a}$ can be realized by choosing

$$\Omega_a(t-t_f)=\Omega(t),\quad \delta_a(t-t_f)=-2\delta(t), \tag{30}$$

and therefore generate the transition

$$\begin{aligned}&\mathcal{N}[\alpha_1|00\rangle_{12}+e^{-i\gamma(t_f)-i\xi(t_f)-i\pi/4}(\alpha_2|0r\rangle_{12}\\ &\quad+\alpha_3|r0\rangle_{12})+\alpha_4|11\rangle_{12}]\otimes|0\rangle_a\\ &\to\frac{1}{\sqrt{2}}\mathcal{N}_1(\alpha_1|00\rangle_{12}+\alpha_4|11\rangle_{12})\otimes e^{-i\gamma(t_f)-i\xi(t_f)-i\pi/4}|r\rangle_a\\ &\quad+\frac{1}{\sqrt{2}}\mathcal{N}_2e^{-i\gamma(t_f)-i\xi(t_f)-i\pi/4}(\alpha_2|0r\rangle_{12}+\alpha_3|r0\rangle_{12})\otimes|0\rangle_a,\end{aligned} \tag{31}$$

with $\mathcal{N}_1=1/(|\alpha_1|^2+|\alpha_4|^2)^{1/2}$ and $\mathcal{N}_2=1/(|\alpha_2|^2+|\alpha_3|^2)^{1/2}$.

Step 3. [for the time interval $t\in(2t_f,3t_f)$] Turn on pulses Ω_1, $\Omega_2(t)$, $\Omega_3(t)$, and $\Omega_4(t)$ of atoms 1 and 2 again, with expressions

$$\Omega_2(t-2t_f)=\overline{\Omega}(t)=-\frac{\dot{\theta}(t_f-t)}{\sin[2\xi(t_f-t)]},$$
$$\Omega_3(t-2t_f)=\begin{cases}\sqrt{\Delta_3\overline{\delta}(t)}, & \overline{\delta}(t)\geqslant 0\\ 0, & \overline{\delta}(t)<0,\end{cases}$$
$$\Omega_4(t-2t_f)=\begin{cases}0, & \overline{\delta}(t)\geqslant 0\\ \sqrt{-\Delta_3\overline{\delta}(t)}, & \overline{\delta}(t)<0.\end{cases} \tag{32}$$

We also plot the Rabi frequencies in $t\in(2t_f,3t_f)$ in Fig. 5(b). Step 3 will result in inverse transition of $\mathcal{X}$, called

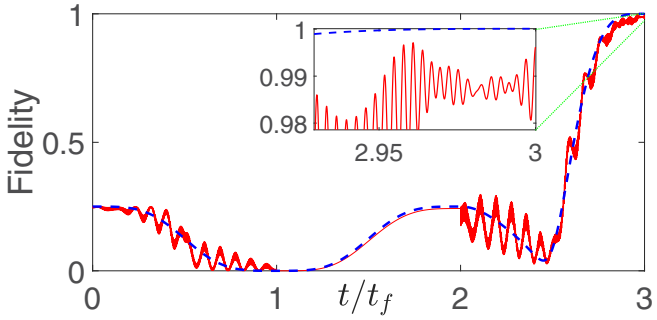

FIG. 6. Fidelities for the NRPM with red solid and blue dotted lines corresponding to original Hamiltonian driving and effective Hamiltonian driving, respectively. The initial and final states are shown in Eqs. (34), and (35), respectively.

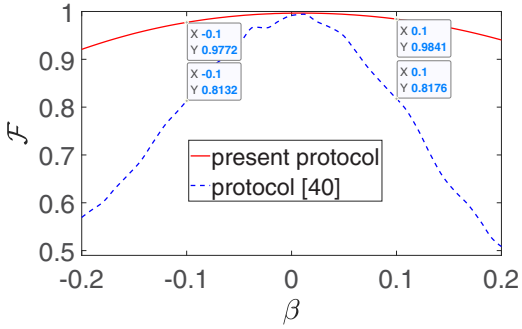

FIG. 7. Fidelity $\mathcal{F}$ vs rate β of systematic errors in Ω_2 and Ω_a, with red solid line and blue dotted line denoting present protocol and the protocol of Ref. [40], respectively. The relevant parameters used to plot the blue dotted line are shown in Fig. 6 of Ref. [40].

$\overline{\mathcal{X}}$, yielding

$$\begin{aligned}&\frac{1}{\sqrt{2}}\mathcal{N}_1(\alpha_1|00\rangle_{12}+\alpha_4|11\rangle_{12})\otimes e^{-i\gamma(t_f)-i\xi(t_f)-i\pi/4}|r\rangle_a\\&\quad+\frac{1}{\sqrt{2}}\mathcal{N}_2 e^{-i\gamma(t_f)-i\xi(t_f)-i\pi/4}(\alpha_2|0r\rangle_{12}\\&\quad+\alpha_3|r0\rangle_{12})\otimes|0\rangle_a\\&\rightarrow\frac{1}{\sqrt{2}}\mathcal{N}_1(\alpha_1|00\rangle_{12}+\alpha_4|11\rangle_{12})\otimes e^{-i\gamma(t_f)-i\xi(t_f)-i\pi/4}|r\rangle_a\\&\quad+\frac{1}{\sqrt{2}}\mathcal{N}_2(\alpha_2|01\rangle_{12}+\alpha_3|10\rangle_{12})\otimes|0\rangle_a.\end{aligned}\tag{33}$$

Recall the term $2(\frac{\Omega_3(t)^2}{\Delta_3}-\frac{\Omega_4(t)^2}{\Delta_3})|11\rangle_{12}\langle 11|$ ignored in Sec. II, which just results in the change of phase of $|11\rangle_{12}$, and we can see from Eq. (33) that whatever phase the term causes in $\mathcal{X}$, the inverse operation $\overline{\mathcal{X}}$ cancels it out.

It is clear that there is no simultaneous excitation of Rydberg atoms during Steps 1–3. Hence the mechanical effect and the further possible ionization are slight. After doing these three steps, we can measure atom a. Result $|0\rangle_a$ corresponds to atoms 1 and 2 now being in $\mathcal{N}_2(\alpha_2|01\rangle_{12}+\alpha_3|10\rangle_{12})$. On the other hand, result $|r\rangle_a$ corresponds to atoms 1 and 2 now being in $\mathcal{N}_1(\alpha_1|00\rangle_{12}+\alpha_4|11\rangle_{12})$. So far, we have constructed the robust and high-fidelity NRPM on atoms 1 and 2.

V. DISCUSSION

We primarily define the initial state

$$|\psi(0)\rangle=\tfrac{1}{2}(|00\rangle_{12}+|01\rangle_{12}+|10\rangle_{12}+|11\rangle_{12})\otimes|0\rangle_a.\tag{34}$$

If the NRPM is successful, we will get a final state as

$$\begin{aligned}|\psi(3t_f)\rangle=&\tfrac{1}{2}(|00\rangle_{12}+|11\rangle_{12})\otimes e^{-i\gamma(t_f)-i\xi(t_f)-i\pi/4}|r\rangle_a\\&+\tfrac{1}{2}(|01\rangle_{12}+|10\rangle_{12})\otimes|0\rangle_a.\end{aligned}\tag{35}$$

First of all, it is appropriate to check veracity of the effective Hamiltonian shown in Eq. (4). So we plot differences between the original Hamiltonian and the effective Hamiltonian versus time in Fig. 6, where we can see that, because of the use of perturbation theory in deriving the effective Hamiltonian, the red solid line, corresponding to the original Hamiltonian, vibrates and approaches the blue dotted line (the original Hamiltonian). The finial point of the red solid line reaches 0.9952, implying the veracity of Eq. (4).

Subsequently, consider the systematic errors in Rabi frequencies $\Omega_2(t)$ and $\Omega_a(t)$, we set

$$\Omega_2^{\rm real}(t)=(1+\beta)\Omega_2(t),\quad \Omega_a^{\rm real}(t)=(1+\beta)\Omega_a(t),\tag{36}$$

where $\Omega_2^{\rm real}(t)$ and $\Omega_a^{\rm real}(t)$ are the experimental values of $\Omega_2(t)$ and $\Omega_a(t)$, respectively. The evolution of system can be described by time-dependent matrix operator $\rho(t)$, given by

$$\dot{\rho}(t)=-i[H^{\rm real}(t),\rho(t)],\tag{37}$$

with $H^{\rm real}(t)$ being the real Hamiltonian of atoms 1, 2, and a [substituting $\Omega_2^{\rm real}(t)$ and $\Omega_a^{\rm real}(t)$ into the total Hamiltonian $H_{\rm tot}=\Omega_a(t)|0\rangle_a\langle r|+{\rm H.c.}+\delta_a(t)|r\rangle_a\langle r|+H_i(t)$], where $H_i(t)$ is shown in Eq. (1), i.e., the original Hamiltonian. We define the fidelity $\mathcal{F}$ for the NRPM as

$$\mathcal{F}={\rm Tr}[\rho(3t_f)|\psi(3t_f)\rangle\langle\psi(3t_f)|].\tag{38}$$

Referring to experimental scheme [65,66], a group of parameters,

$$\begin{aligned}&V=\Delta_1=2\pi\times 50\ {\rm MHz},\quad t_f=6.37\ \mu{\rm s},\\&\Omega_1=23.56\ {\rm MHz},\end{aligned}\tag{39}$$

is chosen here. Note that the values of $\Omega_2(t)$, $\Omega_3(t)$, $\Omega_4(t)$, $\Omega_a(t)$, and $\delta_a(t)$ can be derived with $t_f=6.37\ \mu$s, yielding

$$\begin{aligned}&\max[|\Omega_2(t)|]=\max[|\Omega_a(t)|]=1.69\ {\rm MHz},\\&\max[|\Omega_3(t)|]=\max[|\Omega_4(t)|]=2.98\ {\rm MHz},\\&\max[|\delta_a(t)|]=0.785\ {\rm MHz}.\end{aligned}\tag{40}$$

In such a situation, the relations between fidelity $\mathcal{F}$ and systematic error rate β [in $\Omega_2(t)$ and $\Omega_a(t)$] in the present protocol and in the protocol of Ref. [40] are plotted in Fig. 7. From Fig. 7 we can see that, because of the optimization of the inverse engineering shown in Sec. II, the fidelity $\mathcal{F}$ in our protocol is still as high as 97.72% (98.41%) when β reaches -0.1 (0.1), but $\mathcal{F}$ in the protocol of Ref. [40] is 81.32% (81.76%) at points $\beta=-0.1$ (0.1) without optimization. Observe that this result is not the same as that shown in Fig. 3 because here we

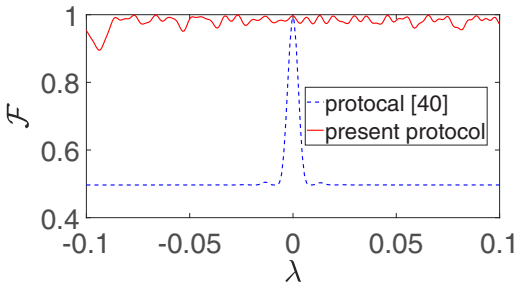

FIG. 8. Fidelity $\mathcal{F}$ vs rate λ of systematic error in V, with blue dotted line and red solid line denoting the protocol of Ref. [40] and the present protocol, respectively. The relevant parameters used to plot the blue dotted line are shown in Fig. 6 of Ref. [40]. Note that the fluctuation of the fidelity in the present protocol is rough because some excitation is arisen to $|D\rangle_{12}$ and $|rr\rangle_{12}$ states due to the systematic error in V.

use the fields $\Omega(t)$ and $\delta(t)$ three times in these three steps. Hence $\mathcal{F}$ is different from the fidelity corresponding to the two-level system. Additionally, the tiny difference between the total Hamiltonian and the effective Hamiltonian will also decrease $\mathcal{F}$.

Similarly, when there is a systematic error with rate λ in interaction strength V, the real value of V in the experiment can be assumed as $V^{\text{real}} = (1+\lambda)V$. Recalling back to the effective Hamiltonian in the protocol of Ref. [40], $H_{\text{eff}} = \frac{\Omega^2}{2\Delta}[|00\rangle\langle RR| + |11\rangle\langle rr|] + \text{H.c.}$ with $V \gg \Omega$, one will find that the deviation of V, λV, can be reserved to the effective Hamiltonian as form $\lambda V(|RR\rangle\langle RR| + |rr\rangle\langle rr|)$ because, generally, $V \gg \lambda V$. Furthermore, λV may have the same magnitude as the effective pulse $\frac{\Omega^2}{2\Delta}$ ($V = 2\Delta$ in the protocol of Ref. [40]), resulting in inefficiencies of the effective Hamiltonian in the protocol of Ref. [40]. Therefore the systematic error in V hugely affects the fidelity of the protocol of Ref. [40]. For example, the fidelity goes down to about 0.5 [see Fig. 6(a) in Ref. [40]] when $\lambda = 5\%$. In contrast, the present protocol will be robust to λV because we avoid simultaneous excitation of Rydberg atoms. A rough explanation is, when similar $\lambda V|rr\rangle\langle rr|$ is added to our effective Hamiltonian $H'_{\text{eff}}(t)$ in Eq. (3), $H'_{\text{eff}}(t)$ will still be valid due to not including $|rr\rangle$. We plot the fidelity $\mathcal{F}$ versus λ in Fig. 8, from which we can see that fidelity in the present protocol is much more robust against that in the protocol of Ref. [40]. When considering $\lambda = 10\%$, the fidelities are 97.06% and 49.65% in the present protocol and in the protocol of Ref. [40], respectively.

On the other side, the thermal noise and the dephasing will induce the decoherence of the system, bringing down the fidelity $\mathcal{F}$. Thereupon, it is appropriate to consider them by utilizing the master equation [67]

$$\dot{\rho}(t) = i[\rho(t),\ H_{\text{tot}}(t)] + D_{\text{de}}[\rho(t)] + D_{\text{th}}[\rho(t)], \tag{41}$$

where $D_{\text{de}}[\rho(t)]$ and $D_{\text{th}}[\rho(t)]$ depend on the dephasing and

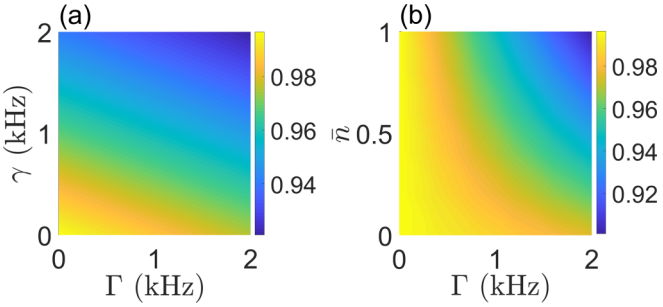

FIG. 9. (a) Fidelity for the NRPM vs the spontaneous emission rate Γ and the dephasing rate γ. (b) Fidelity for the NRPM vs the spontaneous emission rate Γ and the average number $\bar{n}$ of thermal phonons.

the thermal noise, respectively, written as

$$D_{\text{de}}[\rho(t)] = \sum_{l=6}^{10}\left[L_l\rho L_l^\dagger - \frac{1}{2}(L_l^\dagger L_l\rho + \rho L_l^\dagger L_l)\right],$$

$$D_{\text{th}}[\rho(t)] = \sum_{l=1}^{5}\left\{(\bar{n}+1)\left[L_l\rho L_l^\dagger - \frac{1}{2}(L_l^\dagger L_l\rho + \rho L_l^\dagger L_l)\right] + \bar{n}\left[L_l^\dagger\rho L_l - \frac{1}{2}(L_l L_l^\dagger\rho + \rho L_l L_l^\dagger)\right]\right\}, \tag{42}$$

with $\bar{n}$ being the average number of thermal phonons, given by the Bose-Einstein distribution $\bar{n} = 1/(e^{\frac{\hbar\omega}{k_B T}} - 1)$ (ω representing the frequency of the thermal noise). It is worth mentioning that, when $\bar{n}$ equals zero, the thermal noise influences the evolution like spontaneous emission does. The Lindblad operator L_l ($l = 1, 2, \ldots, 10$) in Eq. (42) can be written as

$$\begin{aligned}
&L_1 = \sqrt{\Gamma_{01}/2}|0\rangle_1\langle r|, \quad L_2 = \sqrt{\Gamma_{02}/2}|0\rangle_2\langle r|,\\
&L_3 = \sqrt{\Gamma_{11}/2}|1\rangle_1\langle r|, \quad L_4 = \sqrt{\Gamma_{12}/2}|1\rangle_2\langle r|,\\
&L_5 = \sqrt{\Gamma_a}|0\rangle_a\langle r|, \quad L_6 = \sqrt{\gamma_1/2}(|r\rangle_1\langle r| - |1\rangle_1\langle 1|),\\
&L_7 = \sqrt{\gamma_2/2}(|r\rangle_2\langle r| - |1\rangle_2\langle 1|),\\
&L_8 = \sqrt{\gamma_1/2}(|r\rangle_1\langle r| - |0\rangle_1\langle 0|),\\
&L_9 = \sqrt{\gamma_2/2}(|r\rangle_2\langle r| - |0\rangle_2\langle 0|),\\
&L_{10} = \sqrt{\gamma_a}(|r\rangle_a\langle r| - |0\rangle_a\langle 0|),
\end{aligned} \tag{43}$$

where $\Gamma_{jk}/2$ and Γ_a ($j = 0, 1$ and $k = 1, 2$) are the spontaneous emission rates of paths $|r\rangle_k \to |j\rangle_k$ and $|r\rangle_a \to |0\rangle_k$, respectively. In addition, γ_p ($p = 1, 2, a$) is the dephasing rate of atom p. For simplicity, we assume $\Gamma_{01} = \Gamma_{02} = \Gamma_{11} = \Gamma_{12} = \Gamma_a = \Gamma$ and $\gamma_1 = \gamma_2 = \gamma_a = \gamma$. Under the same conditions of parameters indicated in Eqs. (39) and (40), we discuss the influence on $\mathcal{F}$ of the thermal noise and the dephasing, in Fig. 9, from which we can find that $\mathcal{F}$ is robust against both thermal noise and dephasing. The range of Γ is closed to experimental observation [68,69], and the range of $\bar{n} =$ 0–1 can be regarded as the temperature scope, 0–68.31 μK (assuming the frequency of the thermal noise is $2\pi \times 1$ MHz). For example, set $\Gamma = \gamma = 1$ kHz and $\bar{n} = 0.2$ (namely, the experimental temperature being 26.81 μK [70]), leading to $\mathcal{F} = 95.02\%$, which is experimentally acceptable.

For a concrete experimental process, we may consider the two-photon excitation process [29,65,71–77] in the Rb atom platform with the corresponding ground-state encoding $|0\rangle \equiv |5S_{1/2}, F = 2, m_F = 0\rangle$, $|1\rangle \equiv |5S_{1/2}, F = 1, m_F = 0\rangle$, and $|r\rangle \equiv |60S_{1/2}, m_j = 1/2\rangle$. The C_6 parameter, van der Waals coefficient of specific Rydberg states, is given by $C_6 = n^{11}(11.97 - 0.8486n + 3.385 \times 10^{-3}n^2)$ in atomic units [78,79] with n representing the principal quantum number. We have $C_6 = 140$ GHz μm^6 h here, and the RRI strength V equals $2\pi \times 50$ MHz ($\hbar = 1$) when the atomic distance is set as 3.75 μm ($V = C_6/d^6$).

VI. CONCLUSION

In summary, we proposed a robust scheme for a NRPM with high fidelity. Specifically, we built a model by using the modified unconventional Rydberg pumping to guarantee that there is no simultaneous excitation of Rydberg atoms during the whole evolution. Furthermore, we utilized optimized inverse engineering against systematic error to design suitable fields for a robust and high-fidelity NRPM. Compared with representative work about NRPMs in Ref. [40], the present scheme has several advantages as follows:

(i) Insensitivity to the mechanical effect. The mechanical effect, which results from simultaneous excitation of Rydberg atoms, which is always an obstacle to the Rydberg-atom based QIP, is almost avoided in the present scheme.

(ii) Tolerance to parameter deviation. By carrying out a numerical simulation, we find that the present scheme is relatively insensitive to systematic error. For example, the fidelities are as high as 97.72% and 98.41% when serious systematic error rates in driving pulses reach -0.1 and 0.1, respectively. In addition, the scheme is robust against the decoherence induced by thermal noise and dephasing, further proving the experimental feasibility.

Ergo, the work has a certain experimental practicability and may increase scalability of the nondestructive parity meter, building a bridge to the Rydberg-atom-based QIP. We hope the scheme can be considered for application in upcoming experiments.

ACKNOWLEDGMENT

This work was supported by the National Natural Science Foundation of China under Grants No. 11575045, No. 11674060, No. 11805036, and No. 11804308.

APPENDIX: DETAILED PROOF FROM EQ. (1) TO EQ. (2)

The Hamiltonian in Eq. (1) can be described by a rotating frame with respect to $U_{\rm rot}(t) = e^{iV|rr\rangle_{12}\langle rr|t}$. That is, the Hamiltonian in the new picture is given by

$$H_i'(t) = U_{\rm rot}(t)H_i(t)U_{\rm rot}^\dagger(t) + i\dot{U}_{\rm rot}(t)U_{\rm rot}^\dagger(t). \tag{A1}$$

By utilizing the condition $V = \Delta_1$, Eq. (A1) can be decomposed into two parts, one with high frequency, and the other being resonant, yielding

$$\begin{aligned} H_{i1}'(t) &= [\Omega_2(t) + \Omega_3(t)e^{i\Delta_3 t} + \Omega_4(t)e^{-i\Delta_4 t}]e^{-i\Delta_1 t} \\ &\quad \times \sqrt{2}|D\rangle_{12}\langle rr| + [\Omega_1 e^{-i\Delta_1 t} + \Omega_3(t)e^{-i\Delta_3 t} \\ &\quad + \Omega_4(t)e^{i\Delta_4 t}](|r0\rangle_{12}\langle 10| + |0r\rangle_{12}\langle 01| \\ &\quad + \sqrt{2}|D\rangle_{12}\langle 11|) + \text{H.c.}, \\ H_{i2}'(t) &= \Omega_2(t)(|r0\rangle_{12}\langle 10| + |0r\rangle_{12}\langle 01| + \sqrt{2}|D\rangle_{12}\langle 11|) \\ &\quad + \sqrt{2}\Omega_1|rr\rangle_{12}\langle D| + \text{H.c.}, \end{aligned} \tag{A2}$$

with $|D\rangle_{12} = (|1r\rangle_{12} + |r1\rangle_{12})/\sqrt{2}$. Rewrite $H_{i1}'(t)$ as $H(t) = \sum_u (h_u e^{-i\omega_u t} + h_u^\dagger e^{i\omega_u t})$ and assume $\Delta_3 = \Delta_4$, yielding

$$\begin{aligned} h_1 &= \sqrt{2}\Omega_2(t)|D\rangle_{12}\langle rr| + \Omega_1(t)(|r0\rangle_{12}\langle 10| \\ &\quad + |0r\rangle_{12}\langle 01| + \sqrt{2}|D\rangle_{12}\langle 11|), \\ h_2 &= \sqrt{2}\Omega_3(t)|D\rangle_{12}\langle rr|, \quad h_3 = \sqrt{2}\Omega_4(t)|D\rangle_{12}\langle rr|, \\ h_4 &= \Omega_3(t)(|r0\rangle_{12}\langle 10| + |0r\rangle_{12}\langle 01| + \sqrt{2}|D\rangle_{12}\langle 11|) \\ &\quad + \Omega_4(t)(|10\rangle_{12}\langle r0| + |01\rangle_{12}\langle 0r| + \sqrt{2}|11\rangle_{12}\langle D|), \end{aligned} \tag{A3}$$

with corresponding frequencies $\omega_1 = \Delta_1$, $\omega_2 = \Delta_1 - \Delta_3$, $\omega_3 = \Delta_1 + \Delta_3$, and $\omega_4 = \Delta_3$, respectively. Subsequently we have [80]

$$H_{\rm eff1}'(t) \approx \sum_u [h_u^\dagger, h_u]/\omega_u, \tag{A4}$$

with $\{u, v\} = \{1, 2, 3, 4\}$. The high-frequency terms, i.e., terms with $e^{-i(\omega_u - \omega_v)t}$ ($\omega_u \neq \omega_v$), $e^{-i(\omega_u + \omega_v)t}$, or $e^{-i\omega_u t}$ possess frequencies, such as $|\Delta_3|$, $|\Delta_1 - \Delta_3|$, $2|\Delta_3|$, $|\Delta_1 - 2\Delta_3|$, and $|\Delta_1|$. Considering the conditions $\Delta_1 \gg \Omega_1 \gg \Omega_2(t)$, $\Delta_3 = \Delta_4$, and $\{\Delta_3, \Delta_1 \pm \Delta_3, \Delta_1 - 2\Delta_3\} \gg \{\Omega_3(t), \Omega_4(t)\}$, the high-frequency terms can be further neglected because their averaged performance over a period of time is close to zero compared with the resonant terms. Equation (A4) gives rise to

$$\begin{aligned} H_{\rm eff1}'(t) &= \left(\frac{\Omega_1^2}{\Delta_1} + \frac{\Omega_3(t)^2}{\Delta_3} - \frac{\Omega_4(t)^2}{\Delta_3}\right) \\ &\quad \times (2|11\rangle_{12}\langle 11| + |01\rangle_{12}\langle 01| + |10\rangle_{12}\langle 10| \\ &\quad - |0r\rangle_{12}\langle 0r| - |r0\rangle_{12}\langle r0| - 2|D\rangle_{12}\langle D|) \\ &\quad + \frac{2\Omega_1\Omega_2(t)}{\Delta_1}(|11\rangle_{12}\langle rr| + \text{H.c.}) \\ &\quad + \left(\frac{2\Omega_2(t)^2}{\Delta_1} + \frac{2\Omega_3(t)^2}{\Delta_1 - \Delta_3} + \frac{2\Omega_4(t)^2}{\Delta_1 + \Delta_3}\right) \\ &\quad \times (|rr\rangle_{12}\langle rr| - |D\rangle_{12}\langle D|). \end{aligned} \tag{A5}$$

Observe that term $\frac{2\Omega_1\Omega_2(t)}{\Delta_1}(|11\rangle_{12}\langle rr| + \text{H.c.})$ can be ignored because of the condition $\Omega_1 \gg \Omega_2(t)$, and afterward makes states $|rr\rangle_{12}$ and $|D\rangle_{12}$ be decoupled from the evolution of system. Therefore, $H_{\rm eff1}'(t)$ can be further derived as

$$\begin{aligned} H_{\rm eff1}'(t) &\approx \left(\frac{\Omega_3(t)^2}{\Delta_3} - \frac{\Omega_4(t)^2}{\Delta_3}\right) \\ &\quad \times (2|11\rangle_{12}\langle 11| + |01\rangle_{12}\langle 01| + |10\rangle_{12}\langle 10| \\ &\quad - |0r\rangle_{12}\langle 0r| - |r0\rangle_{12}\langle r0|), \end{aligned} \tag{A6}$$

via introducing the other ancillary pulse Ω_1' with opposite red detuning Δ_1, i.e., canceling the Stark-shift terms in Ω_1.

Additionally, by rotating into another picture with transformation $U'_{\rm rot}(t) = \exp[i\sqrt{2}\Omega_1 t(|rr\rangle_{12}\langle D| + \text{H.c.})]$, we can simplify the resonant part of the original Hamiltonian as

$$\begin{aligned} H''_{i2}(t) = {} & \Omega_2(t)(|r0\rangle_{12}\langle 10| + |0r\rangle_{12}\langle 01|) \\ & + \sqrt{2}\Omega_2(t)[i\sin(\sqrt{2}\Omega_1 t)|rr\rangle_{12}\langle 11| \\ & + \cos(\sqrt{2}\Omega_1 t)|D\rangle_{12}\langle 11|] + \text{H.c.} \end{aligned} \tag{A7}$$

Note that high-frequency terms in Eq. (A5) can be further refined as $(\frac{\Omega_2(t)^2}{\sqrt{2}\Omega_1}|rr\rangle_{12}\langle D| + \text{H.c.})$ by second-order perturbation theory, apparently being decoupled with the evolution of system. Therefore, the effective value of $H''_{i2}(t)$ is

$$H''_{\rm eff2}(t) = \Omega_2(t)(|r0\rangle_{12}\langle 10| + |0r\rangle_{12}\langle 01|) + \text{H.c.} \tag{A8}$$

It is worth mentioning that $H''_{\rm eff2}(t)$ is in a different picture than $H'_{\rm eff1}(t)$. However, the picture transformation operator $U'_{\rm rot}(t)$ cannot change basis $\{|r0\rangle_{12}, |10\rangle_{12}, |0r\rangle_{12}, |01\rangle_{12}\}$, and hence leads to $H'_{\rm eff2}(t) = H''_{\rm eff2}(t)$.

Thereupon, the total effective Hamiltonian is given by

$$\begin{aligned} H'_{\rm eff}(t) = {} & \Omega_2(t)(|r0\rangle_{12}\langle 10| + |0r\rangle_{12}\langle 01|) + \text{H.c.} \\ & + \left(\frac{\Omega_3(t)^2}{\Delta_3} - \frac{\Omega_4(t)^2}{\Delta_3}\right) \\ & \times (2|11\rangle_{12}\langle 11| + |01\rangle_{12}\langle 01| + |10\rangle_{12}\langle 10| - |0r\rangle_{12} \\ & \times \langle 0r| - |r0\rangle_{12}\langle r0|). \end{aligned} \tag{A9}$$

[1] J. W. Pan, C. Simon, C. Brukner, and A. Zeilinger, Nature (London) **410**, 1067 (2001).
[2] C. W. J. Beenakker, D. P. DiVincenzo, C. Emary, and M. Kindermann, Phys. Rev. Lett. **93**, 020501 (2004).
[3] K. Nemoto and W. J. Munro, Phys. Rev. Lett. **93**, 250502 (2004).
[4] H. A. Engel and D. Loss, Science **309**, 586 (2005).
[5] B. S. Shi and A. Tomita, Phys. Lett. A **296**, 161 (2002).
[6] Y. Xia, C. B. Fu, S. Zhang, K. H. Yeon, and C. I. Um, J. Korean Phys. Soc. **46**, 388 (2005).
[7] L. H. Jin, X. R. Jin, and S. Zhang, Phys. Rev. A **72**, 024305 (2005).
[8] K. Azuma, H. Takeda, M. Koashi, and N. Imoto, Phys. Rev. A **85**, 062309 (2012).
[9] X. W. Wang, S. Q. Tang, L. J. Xie, and D. Y. Zhang, Opt. Commun. **296**, 153 (2013).
[10] S. B. van Dam, J. Cramer, T. H. Taminiau, and R. Hanson, Phys. Rev. Lett. **123**, 050401 (2019).
[11] M. D. Lukin, M. Fleischhauer, R. Cote, L. M. Duan, D. Jaksch, J. I. Cirac, and P. Zoller, Phys. Rev. Lett. **87**, 037901 (2001).
[12] D. Jaksch, J. I. Cirac, P. Zoller, S. L. Rolston, R. Côté, and M. D. Lukin, Phys. Rev. Lett. **85**, 2208 (2000).
[13] M. Saffman, T. G. Walker, and K. Mølmer, Rev. Mod. Phys. **82**, 2313 (2010).
[14] M. Saffman, J. Phys. B: At., Mol. Opt. Phys. **49**, 202001 (2016).
[15] D. Comparat and P. Pillet, J. Opt. Soc. Am. B **27**, A208 (2010).
[16] E. Urban, T. A. Johnson, T. Henage, L. Isenhower, D. Yavuz, T. Walker, and M. Saffman, Nat. Phys. **5**, 110 (2009).
[17] A. Gaëtan, Y. Miroshnychenko, T. Wilk, A. Chotia, M. Viteau, D. Comparat, P. Pillet, A. Browaeys, and P. Grangier, Nat. Phys. **5**, 115 (2009).
[18] C. Ates, T. Pohl, T. Pattard, and J. M. Rost, Phys. Rev. Lett. **98**, 023002 (2007).
[19] T. Amthor, C. Giese, C. S. Hofmann, and M. Weidemüller, Phys. Rev. Lett. **104**, 013001 (2010).
[20] Z. Zuo and K. Nakagawa, Phys. Rev. A **82**, 062328 (2010).
[21] T. E. Lee, H. Häffner, and M. C. Cross, Phys. Rev. Lett. **108**, 023602 (2012).
[22] W. Li, C. Ates, and I. Lesanovsky, Phys. Rev. Lett. **110**, 213005 (2013).
[23] S.-L. Su, E. Liang, S. Zhang, J. J. Wen, L. L. Sun, Z. Jin, and A. D. Zhu, Phys. Rev. A **93**, 012306 (2016).
[24] X. F. Shi, Phys. Rev. Appl. **7**, 064017 (2017).
[25] D. Møller, L. B. Madsen, and K. Mølmer, Phys. Rev. Lett. **100**, 170504 (2008).
[26] D. Barredo, S. Ravets, H. Labuhn, L. Béguin, A. Vernier, F. Nogrette, T. Lahaye, and A. Browaeys, Phys. Rev. Lett. **112**, 183002 (2014).
[27] Y. H. Kang, Y. H. Chen, Z. C. Shi, B. H. Huang, J. Song, and Y. Xia, Phys. Rev. A **97**, 042336 (2018).
[28] M. Saffman and K. Mølmer, Phys. Rev. Lett. **102**, 240502 (2009).
[29] X. L. Zhang, L. Isenhower, A. T. Gill, T. G. Walker, and M. Saffman, Phys. Rev. A **82**, 030306(R) (2010).
[30] S. Möbius, M. Genkin, A. Eisfeld, S. Wüster, and J. M. Rost, Phys. Rev. A **87**, 051602(R) (2013).
[31] D. D. Bhaktavatsala Rao and K. Mølmer, Phys. Rev. Lett. **111**, 033606 (2013).
[32] X. Q. Shao, J. H. Wu, X. X. Yi, and Gui-Lu Long, Phys. Rev. A **96**, 062315 (2017).
[33] A. W. Carr and M. Saffman, Phys. Rev. Lett. **111**, 033607 (2013).
[34] S. L. Su, Q. Guo, H. F. Wang, and S. Zhang, Phys. Rev. A **92**, 022328 (2015).
[35] D. X. Li, X. Q. Shao, J. H. Wu, and X. X. Yi, Opt. Lett. **43**, 1639 (2018).
[36] J. Song, C. Li, Z. J. Zhang, Y. Y. Jiang, and Y. Xia, Phys. Rev. A **96**, 032336 (2017).
[37] Y. Wang, C. S. Hu, Z. C. Shi, B. H. Huang, J. Song, and Y. Xia, Ann. Phys. (Berlin, Ger.) **531**, 1900006 (2019).
[38] A. Omran, H. Levine, A. Keesling, G. Semeghini, T. T. Wang, S. Ebadi, H. Bernien, A. S. Zibrov, H. Pichler, S. Choi *et al.*, Science **365**, 570 (2019).
[39] A. W. Glaetzle, R. M. van Bijnen, P. Zoller, and W. Lechner, Nat. Commun. **8**, 15813 (2017).
[40] S. L. Su, F. Q. Guo, L. Tian, X. Y. Zhu, L. L. Yan, E. J. Liang, and M. Feng, Phys. Rev. A **101**, 012347 (2020).
[41] W. Li, P. J. Tanner, and T. F. Gallagher, Phys. Rev. Lett. **94**, 173001 (2005).

[42] T. Amthor, M. Reetz-Lamour, S. Westermann, J. Denskat, and M. Weidemuller, Phys. Rev. Lett. **98**, 023004 (2007).
[43] T. Amthor, M. Reetz-Lamour, C. Giese, and M. Weidemuller, Phys. Rev. A **76**, 054702 (2007).
[44] D. X. Li and X. Q. Shao, Phys. Rev. A **98**, 062338 (2018).
[45] E. S. Kyoseva and N. V. Vitanov, Phys. Rev. A **73**, 023420 (2006).
[46] P. A. Ivanov, E. S. Kyoseva, and N. V. Vitanov, Phys. Rev. A **74**, 022323 (2006).
[47] N. V. Vitanov, Phys. Rev. A **85**, 032331 (2012).
[48] B. Rousseaux, S. Guerin, and N. V. Vitanov, Phys. Rev. A **87**, 032328 (2013).
[49] Y. C. Li, D. Martínez-Cercós, S. Martínez-Garaot, X. Chen, and J. G. Muga, Phys. Rev. A **97**, 013830 (2018).
[50] Y. H. Kang, Y. H. Chen, Z. C. Shi, B. H. Huang, J. Song, and Y. Xia, Phys. Rev. A **97**, 033407 (2018).
[51] Y. H. Kang, Z. C. Shi, B. H. Huang, J. Song, and Y. Xia, Phys. Rev. A **100**, 012332 (2019).
[52] R. H. Zheng, Y. H. Kang, D. Ran, Z. C. Shi, and Y. Xia, Phys. Rev. A **101**, 012345 (2020).
[53] X. Chen and J. G. Muga, Phys. Rev. A **86**, 033405 (2012).
[54] S. González-Resines, D. Guéry-Odelin, A. Tobalina, I. Lizuain, E. Torrontegui, and J. G. Muga, Phys. Rev. Appl. **8**, 054008 (2017).
[55] D. Guéry-Odelin, A. Ruschhaupt, A. Kiely, E. Torrontegui, S. Martínez-Garaot, and J. G. Muga, Rev. Mod. Phys. **91**, 045001 (2019).
[56] S. Ibáñez, X. Chen, and J. G. Muga, Phys. Rev. A **87**, 043402 (2013).
[57] E. Torrontegui, S. Martínez-Garaot, and J. G. Muga, Phys. Rev. A **89**, 043408 (2014).
[58] B. H. Huang, Y. H. Kang, Y. H. Chen, Q. C. Wu, J. Song, and Y. Xia, Phys. Rev. A **96**, 022314 (2017).
[59] B. H. Huang, Y. H. Kang, Y. H. Chen, Z. C. Shi, J. Song, and Y. Xia, Phys. Rev. A **97**, 012333 (2018).
[60] A. Ruschhaupt, X. Chen, D. Alonso, and J. G. Muga, New J. Phys. **14**, 093040 (2012).
[61] X. T. Yu, Q. Zhang, Y. Ban, and X. Chen, Phys. Rev. A **97**, 062317 (2018).
[62] D. Daems, A. Ruschhaupt, D. Sugny, and S. Guérin, Phys. Rev. Lett. **111**, 050404 (2013).
[63] L. Van Damme, Q. Ansel, S. J. Glaser, and D. Sugny, Phys. Rev. A **95**, 063403 (2017).
[64] L. Van-Damme, D. Schraft, G. T. Genov, D. Sugny, T. Halfmann, and S. Guérin, Phys. Rev. A **96**, 022309 (2017).
[65] T. Wilk, A. Gaëtan, C. Evellin, J. Wolters, Y. Miroshnychenko, P. Grangier, and A. Browaeys, Phys. Rev. Lett. **104**, 010502 (2010).
[66] M. J. Hartmann, F. G. S. L. Brandão, and M. B. Plenio, Nat. Phys. **2**, 849 (2006).
[67] I. Medina and F. L. Semião, Phys. Rev. A **100**, 012103 (2019).
[68] X. F. Zhang, Q. Sun, Y. C. Wen, W. M. Liu, S. Eggert, and A. C. Ji, Phys. Rev. Lett. **110**, 090402 (2013).
[69] S. L. Su, Y. Z. Tian, H. Z. Shen, H. P. Zang, E. J. Liang, and S. Zhang, Phys. Rev. A **96**, 042335 (2017).
[70] J. D. Pritchard, D. Maxwell, A. Gauguet, K. J. Weatherill, M. P. A. Jones, and C. S. Adams, Phys. Rev. Lett. **105**, 193603 (2010).
[71] L. Isenhower, E. Urban, X. L. Zhang, A. T. Gill, T. Henage, T. A. Johnson, T. G. Walker, and M. Saffman, Phys. Rev. Lett. **104**, 010503 (2010).
[72] K. M. Maller, M. T. Lichtman, T. Xia, Y. Sun, M. J. Piotrowicz, A. W. Carr, L. Isenhower, and M. Saffman, Phys. Rev. A **92**, 022336 (2015).
[73] Y. Zeng, P. Xu, X. He, Y. Liu, M. Liu, J. Wang, D. J. Papoular, G. V. Shlyapnikov, and M. Zhan, Phys. Rev. Lett. **119**, 160502 (2017).
[74] C. J. Picken, R. Legaie, K. McDonnell, and J. D. Pritchard, Quantum Sci. Technol. **4**, 015011 (2018).
[75] H. Levine, A. Keesling, A. Omran, H. Bernien, S. Schwartz, A. S. Zibrov, M. Endres, M. Greiner, V. Vuletić, and M. D. Lukin, Phys. Rev. Lett. **121**, 123603 (2018).
[76] H. Levine, A. Keesling, G. Semeghini, A. Omran, T. T. Wang, S. Ebadi, H. Bernien, M. Greiner, V. Vuletić, H. Pichler, and M. D. Lukin, Phys. Rev. Lett. **123**, 170503 (2019).
[77] T. M. Graham, M. Kwon, B. Grinkemeyer, Z. Marra, X. Jiang, M. T. Lichtman, Y. Sun, M. Ebert, and M. Saffman, Phys. Rev. Lett. **123**, 230501 (2019).
[78] K. Singer, J. Stanojevic, M. Weidemüller, and R. Côté, J. Phys. B: At., Mol. Opt. Phys. **38**, S295 (2005).
[79] D. Cano and J. Fortágh, Phys. Rev. A **89**, 043413 (2014).
[80] D. F. V. James and J. Jerke, Can. J. Phys. **85**, 625 (2007).